Monolayer Boron Nitride: Hyperspectral Imaging in the Deep Ultraviolet

Adrien Rousseau, Lei Ren, Alrik Durand, Pierre Valvin, Bernard Gil, Kenji Watanabe, Takashi Taniguchi, Bernhard Urbaszek, Xavier Marie, Cédric Robert, et al.

Monolayer boron nitride: hyperspectral imaging in the deep-ultraviolet

Adrien Rousseau,[†] Lei Ren,[‡] Alrik Durand,[†] Pierre Valvin,[†] Bernard Gil,[†] Kenji Watanabe,[¶] Takashi Taniguchi,[§] Bernhard Urbaszek,[‡] Xavier Marie,[‡] Cédric Robert,[‡] and Guillaume Cassabois*[,†]

†*Laboratoire Charles Coulomb, UMR5221 CNRS-Université de Montpellier, 34095 Montpellier, France*

‡*Université de Toulouse, INSA-CNRS-UPS, LPCNO, 135 Av. Rangueil, 31077 Toulouse, France*

¶*Research Center for Functional Materials, National Institute for Materials Science, 1-1 Namiki, Tsukuba 305-0044, Japan*

§*International Center for Materials Nanoarchitectonics, National Institute for Materials Science, 1-1 Namiki, Tsukuba 305-0044, Japan*

E-mail: guillaume.cassabois@umontpellier.fr

Abstract

The optical response of 2D materials and their heterostructures is the subject of intense research with advanced investigation of the luminescence properties in devices made of exfoliated flakes of few- down to one-monolayer thickness. Despite its prevalence in 2D materials research, hexagonal boron nitride (hBN) remains unexplored in this ultimate regime because of its ultrawide bandgap of about 6 eV and the technical difficulties related to performing microscopy in the deep-ultraviolet domain. Here we report hyperspectral imaging at wavelengths around 200 nm in exfoliated hBN at low

temperature. In monolayer boron nitride we observe direct-gap emission around 6.1 eV. In marked contrast to transition metal dichalcogenides, the photoluminescence signal is intense in few-layer hBN, a result of the near unity radiative efficiency in indirect-gap multilayer hBN.

Introduction

After the advent of graphene,[1] the isolation of atomically-thin layers of transition metal dichalcogenides (TMDs) has opened a novel avenue in solid state physics with a new type of direct bandgap semiconductors.[2–5] The indirect-direct crossover of the bandgap at the monolayer (ML) limit is an ubiquitous signature in TMDs. Stacking and combining various 2D materials was further recognized as an amazing resource enlarging the study of atomic MLs to their van der Waals heterostructures.[6]

In 2D materials research, hexagonal boron nitride (hBN) is a key compound. With an ultrawide bandgap of $\sim$6 eV,[7,8] hBN is used as an ideal 2D insulator, an excellent substrate for graphene and the best barrier material in van der Waals heterostructures. hBN is also emerging as an exciting material in its own right, offering novel material properties that enable a broad range of optical, electro-optical and quantum optics functionalities in various spectral domains.[9,10] It is a natural hyperbolic material in the mid-infrared range, it hosts defects that can be engineered to obtain room-temperature, single-photon emission in the ultraviolet, visible and near-infrared ranges, and it exhibits exceptional properties in the deep-ultraviolet (deep-UV) for a new generation of emitters and detectors in the UV-C.[11] Interestingly, in contrast to TMDs, both the ML and the bulk phases have remarkable opto-electronic properties in the case of hBN, particularly regarding the intense emission of bulk hBN despite the indirect nature of its bandgap.[9]

As for the first demonstration of a direct bandgap in ML MoS_2,[3,4] optical spectroscopy in 2D materials largely relies on microscopy in samples fabricated by exfoliation of bulk lamellar crystals. However hBN is notably absent from the list. This stems from its ultrawide bandgap

of about 6 eV and the technical difficulties related to performing optical microscopy in the deep-UV domain around 200 nm. Cathodoluminescence is a powerful alternative technique with the advantages of reaching an excitation spot down to tens of nm[12] and of relying on a high-energy excitation fully appropriate for ultrawide bandgap semiconductors.[13,14] Still cathodoluminescence was proven to be of limited use for the study of few-layer (FL) hBN samples, resolving the emission spectrum down to six MLs only[15] because of intrinsic limitations of cathodoluminescence for atomically-thin layers. Recent studies have reported significant achievements in spatially-resolved photoluminescence (PL) spectroscopy in the deep-UV by means of either near-field[16] or far-field[17,18] optical microscopes.

Here we use hyperspectral imaging around 200 nm in a scanning confocal PL cryomicroscope[18] to study an exfoliated hBN flake down to the single ML limit. In ML BN we observe direct-gap emission around 6.1 eV, reproducing in ML BN exfoliated from a macroscopic crystal the results obtained in ML BN epitaxially grown on graphite by high temperature molecular beam epitaxy (MBE).[19] In the ML limit, thanks to our spatially-resolved measurements, we further show the suppression of the PL signal around 5.5 eV that arises from excitons bound to stacking faults in multilayer hBN. In FL area the direct-indirect crossover of the bandgap leads to a PL spectrum consisting of the documented series of phonon-assisted recombination lines usually detected in bulk hBN. In marked contrast to TMDs we detect an intense PL signal in FL hBN despite the indirect nature of their bandgap, a result of the near unity radiative efficiency in indirect-gap multilayer hBN. We reveal the relative intensity of the phonon replicas depends on the hBN thickness while maintaining the overall aspect of the emission spectrum in bulk hBN. Our work opens the way to investigate the optical properties of hBN-based twistronic devices with many interesting phenomena to address such as moiré effects, flat bands, and ferroelectricity.

Results and discussion

Exfoliated hBN flake

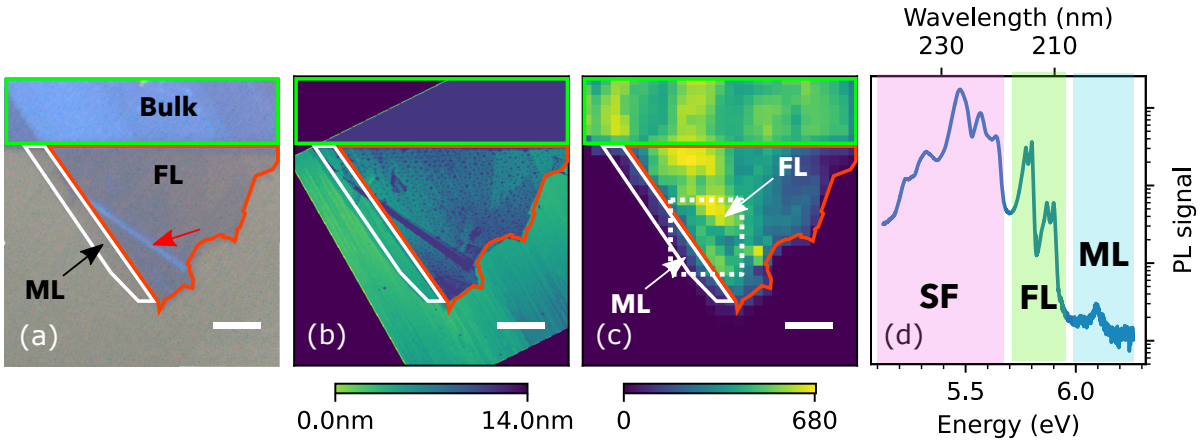

Figure 1: hBN flake exfoliated from a bulk crystal: (a) widefield image in the visible domain, (b) AFM topography, (c) photoluminescence raster scan in the deep-ultraviolet [208<λ<217 nm, i.e. region FL in (d)] recorded at 6 K. Scale bar = 4 μm. The solid lines in (a-c) are guides for the eyes indicating the border of monolayer (white), multilayer (red) and bulk-like (green) hBN regions in the exfoliated flake. (d) Photoluminescence spectrum spatially integrated in the 8×8 μm^2 region indicated by the dotted box in (c). ML stands for monolayer BN, FL for few-layer hBN, and SF for stacking faults.

hBN flakes are mechanically exfoliated from a bulk hBN crystal grown by the high-pressure high-temperature (HPHT) method[7] and then transferred onto a silicon wafer covered by 85 nm silicon oxide (see Methods). Fig.1(a) is a widefield microscope image of the studied flake taken with a white light. Different thicknesses are identified from the optical contrast. Thick bulk-like hBN and FL hBN correspond to the darkest regions, delimitated by green and red lines, respectively [Fig.1(a-c)]. A ML of hBN (delimitated by the white line) is identified through its weaker optical contrast, around 2-3% for this SiO_2 thickness as shown in Ref. 20, and checked with a reference sample where the optical contrast of a well-characterized ML of hBN provides an etalon. Additional information on the sample topography is provided by atomic force microcopy (AFM) (see Methods). In Fig.1(b) the

height difference between the bare substrate and the hBN flake is larger than ∼13 nm in the bulk-like part of the sample, and it varies from 4 to 7 nm in the FL one, except for a line highlighted by a red arrow in Fig.1(a) that may correspond to a folded flake (height ∼12 nm). The spatial variations of the height difference measured by AFM match with the variations of the optical contrast, as indicated by the green and red lines in panels (a) and (b) of Fig.1. Note that the height difference measured between the SiO_2 substrate and the hBN ML is larger (around 2 nm, see line-profile in Fig.4) than the interlayer distance in bulk hBN (0.33 nm) due to a thin contamination or water layer between the SiO_2 surface and hBN.[20] In the FL region, except for the dark line, the layers number has an upper bound varying from 6 to 15 MLs.

A map of the PL signal emitted in the deep-UV is plotted in Fig.1(c). This image corresponds to the spatial variations of the PL signal recorded at 6 K with our scanning confocal deep-UV PL cryomicroscope (see Methods).[18] The excitation energy is 6.39 eV (194 nm) and the PL signal displayed in Fig.1(c) is integrated over the detection window labelled FL in Fig.1(d) (green shaded area) ranging from 5.71 to 5.95 eV ($208<\lambda<217$ nm). In this spectral domain the PL spectrum consists of the intrinsic emission lines due to phonon-assisted recombination in indirect-gap multilayer hBN.[8,9,21–23] The PL map aligns with the widefield image and AFM topography [see green and red lines in Fig.1], providing a first characterization with moderate resolution (800 nm-pixel size) of our exfoliated hBN flake in the deep-UV.

Fig.1(d) displays the PL spectrum spatially-integrated over the 8×8 μm^2 region indicated by the dotted box in Fig.1(c). We highlight three spectral domains of interest in the deep-UV optical response of hBN. In addition to the intrinsic phonon replicas in multilayer hBN already mentioned above [green shaded area, labelled FL in Fig.1(c)], the signal below 5.7 eV [pink shaded area, labelled SF in Fig.1(c)] arises from the recombination of excitons localized at extended defects and stacking faults, as demonstrated by cathodoluminescence measurements in a transmission electron microscope combined with ab initio calculations.[12]

Most of the lines in the SF spectral domain stem from intervalley scattering assisted by the emission of TO phonons at the K point of the Brillouin zone.[24] Although the efficiency of phonon-assisted processes decreases with the number of involved phonons, the emission of up to three TO(K) phonons can give rise to a bright luminescence signal at 5.3 eV [Fig.1(d)]. This is due to the density of final states provided by the stacking faults in multilayer hBN that make intervalley scattering a resonant process.[24] The third spectral domain of interest is the high-energy part of the PL spectrum, above 5.97 eV, labelled ML and displayed as a blue shaded area in Fig.1(d). The line at ∼6.1 eV is the emission from ML BN area, as first revealed by reflectivity and PL in ML BN epitaxially grown on graphite by high temperature MBE.[19] In the latter reference, PL measurements were performed with a standard macro-PL setup, prior to the development of our scanning confocal deep-UV PL cryomicroscope. The emission from ML BN was resolved thanks to the scalable fabrication of hBN with atomic thickness control in high-temperature MBE.[19] Eventually, we point out that the PL spectrum is displayed over four decades in the semi-log scale of Fig.1(d). Since ML BN covers ∼20% of the surface inside the dotted box in Fig.1(c), it is a first indication that the PL signal from a single ML of hBN is not higher than in multilayer hBN. This result is in strong contrast to TMDs[3–5] where a ML is identified from its intense emission due to its direct gap characteristics when performing PL spectroscopy in exfoliated flakes of various thicknesses. Conversely, it provides evidence for a bright luminescence in multilayer hBN despite the indirect nature of the bandgap, an effect reminiscent of the near unity radiative efficiency in bulk hBN,[7,25] further discussed below.

Hyperspectral imaging in the deep-ultraviolet

Fig.2 presents hyperspectral imaging with higher spatial resolution in the region delimitated by the dotted box in Fig.1(c). Panels (a-c) display the spatial variations of the PL signal intensity integrated in three spectral domains: below 5.76 eV (a), in between 5.76 and

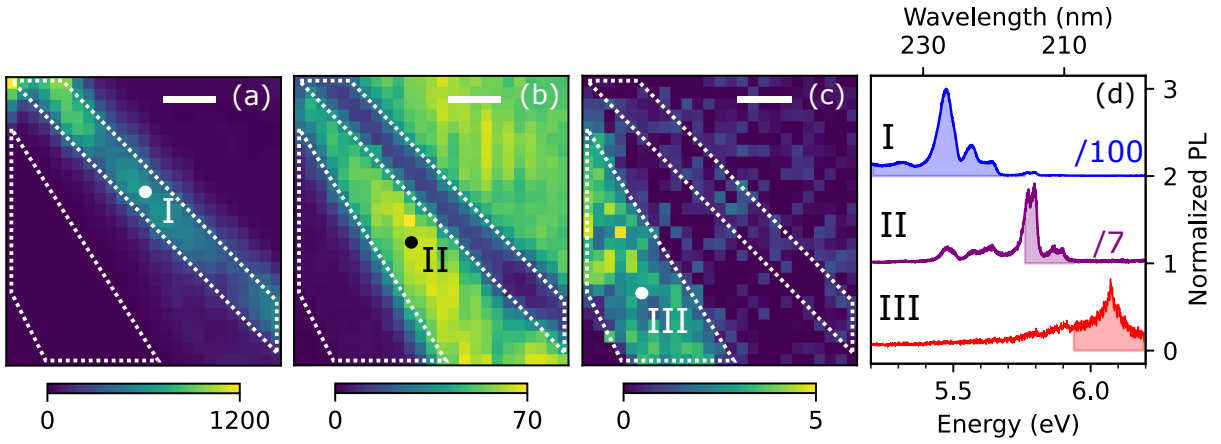

Figure 2: Hyperspectral imaging at 6 K in the region indicated by the dotted box in Fig.1(c). (a-c): maps of the PL signal intensity for energies below 5.76 eV (a), in between 5.76 and 5.93 eV (b), and above 5.93 eV (c), as highlighted in panel (d). Scale bar = 1.6 μm. The dotted lines are guides for the eyes. (d): typical PL spectra detected at three different locations marked in (a-c). (I) is dominated by the recombination at hBN stacking faults, (II) by the intrinsic phonon replicas in indirect-gap multilayer hBN, and (III) by the emission of monolayer BN.

5.93 eV (b), and above 5.93 eV (c), as highlighted in panel (d). Typical PL spectra detected at three different locations marked in panels (a-c) are displayed in Fig.2(d). Spectrum (I) corresponds to the recombination of excitons localized at hBN stacking faults. This PL signal is intense in a $\sim$1 μm-large stripe crossing diagonally in Fig.2(a). This is the line observable in the widefield image and AFM topography in Fig.1. Spectrum (II) is dominated by the intrinsic phonon replicas in indirect-gap multilayer hBN [Fig.2(b)]. This signal is spatially anti-correlated to the defect-related emission in Fig.2(a), in agreement with previous work by cathodoluminescence.[12] In defect-free areas, the PL signal is more or less spatially uniform, as expected for the intrinsic phonon-assisted recombination of delocalized indirect excitons in multilayer hBN. On the contrary, any extended defect and stacking fault opens non-radiative relaxation channels that compete with the intrinsic phonon replicas and strongly reduce their intensity [as shown by spectra (I) and (II) in Fig.2(d)], resulting in the anti-correlation of the PL maps in panels (a) and (b).

Thanks to our scanning confocal PL cryomicroscope operating in the deep-UV, we unveil

the intrinsic emission of a single ML exfoliated from a hBN crystal. This regime has been so far inaccessible to cathodoluminescence experiments. In Fig.2(a-c) the PL signal detected above 5.93 eV appears spatially anti-correlated to the stacking faults emission and to the intrinsic phonon replicas. Importantly, the weak signal centered at ∼6.1 eV is not detected outside the region identified as being a ML from the optical contrast and AFM topography [Fig.1]. Spectrum (III) is the genuine emission spectrum of ML BN in the deep-UV, confirming the results of Ref. 19 based on a radically different fabrication technique and studied with a different setup. The characteristic quadruplet of multilayer and bulk hBN with the intense doublet at ∼5.75 eV [spectrum (II), Fig.2(d)] is not observed in the ML region. Moreover, there is no trace of the broad defect-related emission coming from stacking faults [spectrum (I), Fig.2(d)]. In fact, the concept of stacking fault becomes meaningless for atomically-thin BN so that no related emission is expected. Still, the absence of emission around 5.3-5.5 eV in ML BN is a strong confirmation for the origin of this PL signal as arising from stacking faults, complementing Ref. 12.

Direct-gap emission in monolayer hBN

As mentioned above, a striking result of our hyperspectral imaging in the deep-UV is the weak emission of ML BN in comparison to multilayer hBN, a phenomenology in strong contrast to the one reported in TMDs.[3–5] Such an effect may appear counter-intuitive with respect to the indirect-direct crossover of the bandgap at the ML limit. In semiconductor physics, the radiative efficiency is known to be small in indirect semiconductors, the most common example being silicon with poor optoelectronic properties for light-emitting devices. Although bulk hBN is an indirect bandgap semiconductor,[8] it is a bright emitter in the deep-UV[7] and the radiative efficiency is of order unity.[25] This means the phonon-assisted recombination time is short enough to bypass non-radiative carrier relaxation, a quite unique situation in semiconductor physics,[9] which has been only recently elucidated.[26] In ML BN the radiative efficiency is also of order unity because of the direct nature of the bandgap,[19]

as recently characterized in Ref. 27, so that the radiative recombination is dominant in the relaxation dynamics of both ML and multilayer hBN. The reason for the weak emission in ML BN stems from the photo-excitation process yielding weak absorption. Because of the screening reduction in a ML, the calculated excitonic binding energy increases in hBN from ∼0.7 eV in the bulk to ∼2 eV in the ML, a record value in 2D materials.[28] The onset of the continuum absorption lies at ∼8 eV, an energy lying in the vacuum UV spectral domain. Consequently, the photo-generation of free electron-hole pair states in the absorption continuum is no longer possible in hBN by means of the fourth harmonic of a cw-mode locked Ti:Sa oscillator (see Methods). The detection of PL in ML BN requires a selective excitation with a laser detuning matching the energy of two LA phonons at the M point.[19] From the ratio of spectra (II) and (III) in Fig.2 we estimate that the phonon-assisted photo-excitation below the free-carrier gap in ML BN has an overall efficiency one to two orders of magnitude lower than the direct photo-generation of carriers in the continuum of free excitons in multilayer hBN.

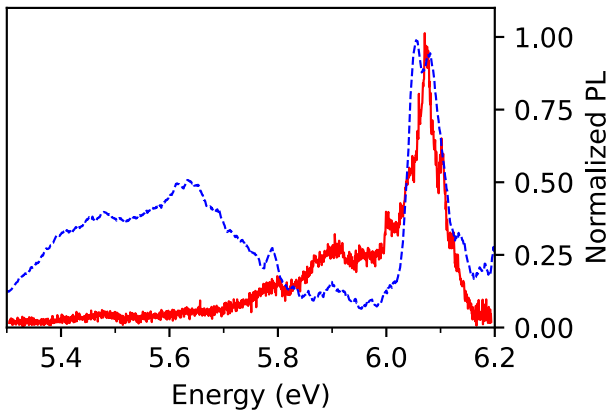

Figure 3: Photoluminescence spectrum of monolayer BN exfoliated from a bulk hBN crystal (red solid line). The signal recorded at 6 K is spatially-integrated in the region labelled ML in Fig.1(a). The blue dotted line shows the photoluminescence spectrum of monolayer BN epitaxially grown on graphite by high temperature MBE, adapted from Ref. 19.

Finally, we compare the PL spectrum of ML BN either exfoliated from a bulk crystal [red

solid line, Fig.3] or epitaxially grown on graphite by high temperature MBE[19] [blue dotted line, Fig.3]. The major difference is the existence of a broad defect-related emission centered at ∼5.5 eV in the hBN epilayer. There are two reasons for this: first the experiments in Ref. 19 were performed with a macro-PL setup (with a laser spot size of ∼50 μm), second the epilayers feature small 3D islands located at the graphite step edges, which serve as nucleation sites for the atomically-thin hBN islands that expand and form a continuous ML in appropriate growth conditions.[29] Consequently, the PL spectrum in Ref. 19 [blue dotted line, Fig.3] is the spatial average of the emission of atomically-flat ML BN and of small bulk-like islands with structural defects. Interesting is the fine structure of the intrinsic emission of ML BN at ∼6.1 eV. In the exfoliated ML [red solid line, Fig.3], in addition to the main peak at 6.07 eV, we resolve narrow secondary maxima at 6.10, 6.04, 6.00 eV together with broader lines at 5.9 and 5.79 eV. Some of these lines were also observed in the epitaxial ML, indicating a complex scenario of the radiative recombination processes. Further study beyond the scope of the present work appears necessary for reaching a detailed understanding of the relaxation dynamics in ML BN.

Indirect-gap emission in few-layer hBN (<15 ML)

In FL hBN we retrieve the PL spectrum reported in bulk hBN.[7,8,21–23,25] As displayed in Fig.2(d) and further detailed in Fig.4(b), the PL signal recorded in the few ML region indicated in Fig.1 is similar to the one of bulk hBN. There is an intense doublet at ∼5.76 eV corresponding to the recombination assisted by LO and TO phonons at the T point of the Brillouin zone, while the doublet at ∼5.86 eV has a lower intensity and comes from LA and TA phonons. We note we do not resolve the 6 meV-fine structure of the phonon replicas arising from overtones of interlayer shear modes, revealed in bulk hBN.[22] This is a consequence of the slightly broader lines detected here in FL hBN.

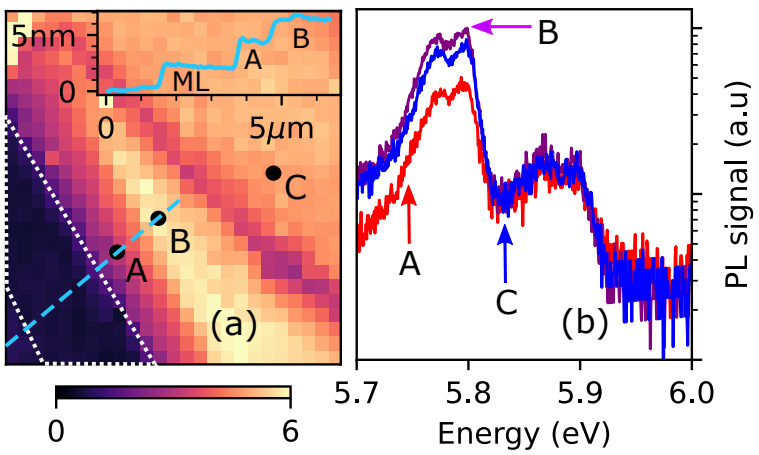

Figure 4: (a) Spatial variations of the intensity ratio of the PL signal emitted in the [5.73-5.83] eV and [5.83-5.93] eV ranges, at 6 K (same region as Fig.2). Inset: line-profile of the AFM topography along the blue dashed line. (b) PL spectra at the A, B and C locations indicated in (a), corresponding to different hBN thickness, as shown in the inset of panel (a). The spectra are normalized to the PL intensity of the LA/TA phonon replicas at ∼5.86 eV.

Particularly striking is the difference of our PL spectra with the rare existing results available in the literature for the deep-UV emission of few nm-thick hBN. In Ref. 15 Schué *et al.* reported cathodoluminescence measurements in exfoliated hBN flakes of reduced thickness, down to 6 MLs (∼2 nm). From 27 to 6 MLs the emission spectrum displays two important modifications with respect to the bulk: first, the doublet of the LA/TA phonon replicas disappears with the observation of a singlet at ∼5.9 eV; second, the latter line is more intense than the emission at ∼5.76 eV coming from the LO/TO phonon replicas. This phenomenology is radically different from the one observed here where the PL spectrum retains the main characteristics that were extensively studied in bulk hBN, as explained above. Such a discrepancy reveals that the deep-UV emission in FL hBN may be sample-dependent. Moreover, we conclude that the PL spectrum in FL hBN can be very similar to the one of bulk hBN, as revealed by our measurements. This suggests the emission reported in Ref. 15 may be the signature of strain-induced effects resulting from the mechanical exfoliation and preparation of the sample. The influence of strain on the optoelectronic properties of hBN in the deep-UV remains unexplored and the disparate results reported here and in Ref. 15

call for an in-depth investigation.

Although our PL spectra resemble the one in bulk hBN, the intensity ratio between the LO/TO phonon replicas and the LA/TA ones is not uniform and depends on the number of MLs, as shown in Fig.4(a) [which corresponds to the same region as in Fig.2]. Importantly, this intensity ratio aligns with the AFM topography. The terrace labelled A has a height of $\sim$4.5 nm, i.e. 2.5 nm thicker than the ML region, setting up an upper bound of 8-9 to the number of MLs at position A. In this terrace, the intensity ratio of the LO/TO to LA/TA PL signal is of the order 3, while it increases to 6 in terrace B of $\sim$6.5 nm-height, with a comparable value in terrace C of similar height. In B and C, the intensity ratio is basically identical to the one measured in bulk hBN.[7,8,25] In terrace A the intensity of the LA/TA phonon replicas increases with respect to the optical phonon replicas. This enhancement of the acoustic phonon replicas in very thin FL hBN is consistent with the results of Schué *et al.*[15] except for the strong deformation of the emission spectrum that we do not observe, as discussed above. Our results motivate a systematic study of this effect for an arbitary number of layers until the ML limit. Our works also paves the way for investigating the influence of a rotation of the hBN layers in the context of twistronics, and in particular the fascinating properties of twisted hBN bilayers,[30–34] by spatially-resolved deep-UV spectroscopy.

Conclusion

We report the first hyperspectral imaging in the deep-UV of few-layer hBN until the ML limit. In ML BN we observe direct-gap emission around 6.1 eV, reproducing in ML BN exfoliated from a macroscopic crystal the results obtained in ML BN epitaxially grown on graphite by high temperature MBE. In marked contrast to transition metal dichalcogenides, the PL signal in ML BN is less intense than in few-layer hBN. This effects stems from the huge excitonic binding energy in ML BN and the corresponding low efficiency of phonon-assisted photo-excitation in ML BN when the excitation laser energy lies below the free-carrier gap. In few-

layer hBN the direct-indirect crossover of the bandgap leads to a PL spectrum consisting of phonon-assisted recombination lines. These phonon replicas are intense, a result reminiscent of the near unity radiative efficiency in indirect-gap multilayer hBN. We reveal the relative intensity of the phonon replicas depends on the hBN thickness while maintaining the overall aspect of the emission spectrum in bulk hBN. Our work opens the perspective to investigate the optical properties of hBN-based twistronic devices with many interesting phenomena to address such as moiré effects, flat bands, and ferroelectricity.

Methods

Sample preparation

We fabricate the sample by mechanical exfoliation of high-quality hBN crystals (grown by the HPHT method). The hBN flake is mechanically exfoliated and deposited onto a 85 nm SiO_2/Si substrate using a dry-stamping technique.[35] Prior to transfer, the substrate is successively cleaned by sonication in aceton and IPA, followed by an O_2/N_2 plasma ashing. No post annealing treatment is performed once the hBN flake is transferred onto the substrate.

AFM characterization

The AFM measurement is conducted with a Nano-Observer (CSI instrument) in ambient environment in tapping mode. The probe (APPNANO, FORT Part # Fort-50) has a radius of less than 10 nm and a frequency of 43-81 kHz.

Deep-ultraviolet scanning confocal cryomicroscope

Deep-ultraviolet hyperspectral cryomicroscopy is performed with the setup described in Ref. 18. Briefly, the excitation is provided by the fourth harmonic of a cw mode-locked Ti:Sa oscillator and it is tunable from 193 nm to 205 nm with trains of 140 fs-pulses at 80 MHz

repetition rate. The injection path uses a series of dielectric mirrors coated for this spectral range. The exciting laser beam is focused by a Schwarzschild objective located inside the closed-cycle cryostat equipped with CaF_2 optical windows. The objective numerical aperture is 0.5, resulting in a laser spot size of 200 nm. The sample is mounted on a stacking of piezoelectric steppers and scanners, that is cooled down to 6 K under ultrahigh vacuum (10^{-11} bar). The photoluminescence is collected by means of an achromatic optical system comprising a pin-hole for confocal filtering. It is then dispersed in a Czerny-Turner spectrometer with 500 mm focal length and a 1200 grooves/mm ruled grating and finally detected by a back-illuminated CCD camera with 13.5 μm pixel size. The corresponding spectral resolution is 0.17 nm (3.3 meV). The whole setup is controlled by homemade Python modules inserted inside the QUDI software suite[36] to create hyperspectral images of the photoluminescence signal recorded at each point of a scanned area. All photoluminescence spectra are normalised to the instrumental response function of the detection system.

Acknowledgement

We gratefully acknowledge C. L'Henoret and T. Cohen for their technical support at the mechanics workshop, P. Beton and S. Novikov for fruitful discussions and critical readings, and B. Lassagne for his help with AFM measurements. This work was financially supported by the network GaNeX (ANR-11-LABX-0014), the BONASPES project (ANR-19-CE30-0007), the ZEOLIGHT project (ANR-19-CE08-0016) and Université de Montpellier. K.W. and T.T. acknowledge support from the Elemental Strategy Initiative conducted by the MEXT, Japan (Grant Number JPMXP0112101001) and JSPS KAKENHI (Grant Numbers 19H05790 and JP20H00354).

References

(1) Novoselov, K. S.; Geim, A. K.; Morozov, S. V.; Jiang, D.; Zhang, Y.; Dubonos, S. V.; Grigorieva, I. V.; Firsov, A. A. Electric Field Effect in Atomically Thin Carbon Films. *Science* **2004**, *306*, 666–669.

(2) Novoselov, K. S.; Jiang, D.; Schedin, F.; Booth, T. J.; Khotkevich, V. V.; Morozov, S. V.; Geim, A. K. Two-dimensional atomic crystals. *Proceedings of the National Academy of Sciences* **2005**, *102*, 10451–10453.

(3) Mak, K. F.; Lee, C.; Hone, J.; Shan, J.; Heinz, T. F. Atomically Thin MoS_2: A New Direct-Gap Semiconductor. *Physical Review Letters* **2010**, *105*, 136805.

(4) Splendiani, A.; Sun, L.; Zhang, Y.; Li, T.; Kim, J.; Chim, C.-Y.; Galli, G.; Wang, F. Emerging Photoluminescence in Monolayer MoS_2. *Nano Letters* **2010**, *10*, 1271–1275.

(5) Wang, G.; Chernikov, A.; Glazov, M. M.; Heinz, T. F.; Marie, X.; Amand, T.; Urbaszek, B. Colloquium: Excitons in atomically thin transition metal dichalcogenides. *Reviews of Modern Physics* **2018**, *90*, 021001.

(6) Geim, A. K.; Grigorieva, I. V. Van der Waals heterostructures. *Nature* **2013**, *499*, 419–425.

(7) Watanabe, K.; Taniguchi, T.; Kanda, H. Direct-bandgap properties and evidence for ultraviolet lasing of hexagonal boron nitride single crystal. *Nature Materials* **2004**, *3*, 404–409.

(8) Cassabois, G.; Valvin, P.; Gil, B. Hexagonal boron nitride is an indirect bandgap semiconductor. *Nature Photonics* **2016**, *10*, 262–266.

(9) Caldwell, J. D.; Aharonovich, I.; Cassabois, G.; Edgar, J. H.; Gil, B.; Basov, D. N. Photonics with hexagonal boron nitride. *Nature Reviews Materials* **2019**, *4*, 552–567.

(10) Gil, B.; Cassabois, G.; Cusco, R.; Fugallo, G.; Artus, L. Boron nitride for excitonics, nano photonics, and quantum technologies. *Nanophotonics* **2020**, *9*, 3483–3504.

(11) Watanabe, K.; Taniguchi, T.; Niiyama, T.; Miya, K.; Taniguchi, M. Far-ultraviolet plane-emission handheld device based on hexagonal boron nitride. *Nature Photonics* **2009**, *3*, 591–594.

(12) Bourrellier, R.; Amato, M.; Galvão Tizei, L. H.; Giorgetti, C.; Gloter, A.; Heggie, M. I.; March, K.; Stéphan, O.; Reining, L.; Kociak, M.; Zobelli, A. Nanometric Resolved Luminescence in h-BN Flakes: Excitons and Stacking Order. *ACS Photonics* **2014**, *1*, 857–862.

(13) Bourrellier, R.; Meuret, S.; Tararan, A.; Stéphan, O.; Kociak, M.; Tizei, L. H. G.; Zobelli, A. Bright UV Single Photon Emission at Point Defects in h-BN. *Nano Letters* **2016**, *16*, 4317.

(14) Hayee, F.; Yu, L.; Zhang, J. L.; Ciccarino, C. J.; Nguyen, M.; Marshall, A. F.; Aharonovich, I.; Vučković, J.; Narang, P.; Heinz, T. F.; Dionne, J. A. Revealing multiple classes of stable quantum emitters in hexagonal boron nitride with correlated optical and electron microscopy. *Nature Materials* **2020**, *19*, 534–539.

(15) Schué, L.; Berini, B.; Betz, A. C.; Plaçais, B.; Ducastelle, F.; Barjon, J.; Loiseau, A. Dimensionality effects on the luminescence properties of hBN. *Nanoscale* **2016**, *8*, 6986–6993.

(16) Ishii, R.; Funato, M.; Kawakami, Y. Pushing the limits of deep-ultraviolet scanning near-field optical microscopy. *APL Photonics* **2019**, *4*, 070801.

(17) Watanabe, K.; Taniguchi, T. Far-UV photoluminescence microscope for impurity domain in hexagonal-boron-nitride single crystals by high-pressure, high-temperature synthesis. *npj 2D Materials and Applications* **2019**, *3*, 1–5.

(18) Valvin, P.; Pelini, T.; Cassabois, G.; Zobelli, A.; Li, J.; Edgar, J. H.; Gil, B. Deep ultraviolet hyperspectral cryomicroscopy in boron nitride: Photoluminescence in crystals with an ultra-low defect density. *AIP Advances* **2020**, *10*, 075025.

(19) Elias, C.; Valvin, P.; Pelini, T.; Summerfield, A.; Mellor, C. J.; Cheng, T. S.; Eaves, L.; Foxon, C. T.; Beton, P. H.; Novikov, S. V.; Gil, B.; Cassabois, G. Direct band-gap crossover in epitaxial monolayer boron nitride. *Nature Communications* **2019**, *10*, 2639.

(20) Gorbachev, R. V.; Riaz, I.; Nair, R. R.; Jalil, R.; Britnell, L.; Belle, B. D.; Hill, E. W.; Novoselov, K. S.; Watanabe, K.; Taniguchi, T.; Geim, A. K.; Blake, P. Hunting for Monolayer Boron Nitride: Optical and Raman Signatures. *Small* **2011**, *7*, 465–468.

(21) Vuong, T. Q. P.; Cassabois, G.; Valvin, P.; Jacques, V.; Lee, A. V. D.; Zobelli, A.; Watanabe, K.; Taniguchi, T.; Gil, B. Phonon symmetries in hexagonal boron nitride probed by incoherent light emission. *2D Materials* **2017**, *4*, 011004.

(22) Vuong, T. Q. P.; Cassabois, G.; Valvin, P.; Jacques, V.; Cuscó, R.; Artús, L.; Gil, B. Overtones of interlayer shear modes in the phonon-assisted emission spectrum of hexagonal boron nitride. *Physical Review B* **2017**, *95*, 045207.

(23) Vuong, T. Q. P.; Liu, S.; Lee, A. V. d.; Cuscó, R.; Artús, L.; Michel, T.; Valvin, P.; Edgar, J. H.; Cassabois, G.; Gil, B. Isotope engineering of van der Waals interactions in hexagonal boron nitride. *Nature Materials* **2018**, *17*, 152.

(24) Cassabois, G.; Valvin, P.; Gil, B. Intervalley scattering in hexagonal boron nitride. *Physical Review B* **2016**, *93*, 035207.

(25) Schué, L.; Sponza, L.; Plaud, A.; Bensalah, H.; Watanabe, K.; Taniguchi, T.; Ducastelle, F.; Loiseau, A.; Barjon, J. Bright Luminescence from Indirect and Strongly Bound Excitons in h-BN. *Physical Review Letters* **2019**, *122*, 067401.

(26) Elias, C.; Fugallo, G.; Valvin, P.; L'Henoret, C.; Li, J.; Edgar, J. H.; Sottile, F.; Lazzeri, M.; Ouerghi, A.; Gil, B.; Cassabois, G. To appear in Phys. Rev. Lett.

(27) Cassabois, G.; Fugallo, G.; Elias, C.; Valvin, P.; Gil, B.; Summerfield, A.; Mellor, C. J.; Cheng, T. S.; Eaves, L.; Foxon, C. T.; Beton, P. H.; Segura, A.; Novikov, S. V. submitted for publication.

(28) Paleari, F.; Galvani, T.; Amara, H.; Ducastelle, F.; Molina-S?nchez, A.; Wirtz, L. Excitons in few-layer hexagonal boron nitride: Davydov splitting and surface localization. *2D Materials* **2018**, *5*, 045017.

(29) Vuong, T. Q. P.; Cassabois, G.; Valvin, P.; Rousseau, E.; Summerfield, A.; Mellor, C. J.; Cho, Y.; Cheng, T. S.; Albar, J. D.; L Eaves,; Foxon, C. T.; Beton, P. H.; Novikov, S. V.; Gil, B. Deep ultraviolet emission in hexagonal boron nitride grown by high-temperature molecular beam epitaxy. *2D Materials* **2017**, *4*, 021023.

(30) Xian, L.; Kennes, D. M.; Tancogne-Dejean, N.; Altarelli, M.; Rubio, A. Multiflat Bands and Strong Correlations in Twisted Bilayer Boron Nitride: Doping-Induced Correlated Insulator and Superconductor. *Nano Letters* **2019**, *19*, 4934–4940.

(31) Ochoa, H.; Asenjo-Garcia, A. Flat Bands and Chiral Optical Response of Moiré Insulators. *Physical Review Letters* **2020**, *125*, 037402.

(32) Zhao, X.-J.; Yang, Y.; Zhang, D.-B.; Wei, S.-H. Formation of Bloch Flat Bands in Polar Twisted Bilayers without Magic Angles. *Physical Review Letters* **2020**, *124*, 086401.

(33) Woods, C. R.; Ares, P.; Nevison-Andrews, H.; Holwill, M. J.; Fabregas, R.; Guinea, F.; Geim, A. K.; Novoselov, K. S.; Walet, N. R.; Fumagalli, L. Charge-polarized interfacial superlattices in marginally twisted hexagonal boron nitride. *Nature Communications* **2021**, *12*, 347.

(34) Yao, K. et al. Enhanced tunable second harmonic generation from twistable interfaces and vertical superlattices in boron nitride homostructures. *Science Advances* **2021**, *7*, eabe8691.

(35) Castellanos-Gomez, A.; Buscema, M.; Molenaar, R.; Singh, V.; Janssen, L.; Zant, H. S. J. v. d.; Steele, G. A. Deterministic transfer of two-dimensional materials by all-dry viscoelastic stamping. *2D Materials* **2014**, *1*, 011002.

(36) QUDI software suite, https://doi.org/10.1016/j.softx.2017.02.001.

Graphical TOC Entry